Received: 9 October 2023 | Revised: 9 October 2023 | Accepted: 15 November 2023

DOI: 10.1002/mawe.202300244

ARTICLE

WILEY VCH

Evaluation of innovative microreactor for examination of alkoxide pitting corrosion and data generation for numerical transient model

Evaluierung eines neuartigen Mikroreaktors für die Untersuchung von Alkoholat-Lochfraßkorrosion und die Datenerzeugung für ein numerisches transientes Modell

V. Arya[1] | **E. Gazenbiller**[2] | **R. Reitz**[1] | **M. Oechsner**[1] | **D. Höche**[2]

[1]Zentrum für Konstruktionswerkstoffe (MPA-IfW) der TU Darmstadt, Darmstadt, Germany

[2]Helmholtz-Zentrum Hereon, Geesthacht, Germany

Correspondence
E. Gazenbiller, Helmholtz-Zentrum Hereon, Max-Planck-Straße 1, 21502 Geesthacht, Germany.
Email: eugen.gazenbiller@hereon.de

Funding information
Deutsche Forschungsgemeinschaft/ German Research Foundation (DFG), Grant/Award Number: DFG HO4478/6-1, OE558/20-1, DFG HO4478/6-2, OE558/20-2

Abstract

In fuel-bearing components, particularly in automotive applications operating at elevated temperatures, the durability of light metals is significantly influenced by their susceptibility to alkoxide corrosion. Alkoxide corrosion is characterized by its spontaneous nature and exceptionally rapid degradation of materials once initiated. This study presents an innovative high-pressure and high-temperature micro-reactor, which enables precise measurements with superior sensitivity for determining the exact initiation times and reaction rates of pitting corrosion. Exemplified tests of surface roughness and water content effect on pitting initiation times were conducted and data was generated for a numerical phase field model to demonstrate the reactor capabilities. Experimental findings suggest that impurities present on both the material surface and in the fuel exhibit a significant influence on corrosivity, thereby affecting the reliability of the components. Moreover, the experimental data points have been utilized to extract the corrosion kinetics and calibrate the numerical model. The initial findings successfully demonstrate the ability to replicate corrosion kinetics and accurately represent pit morphologies and estimate reaction-related parameters in a predictive manner.

KEYWORDS
aluminium alloy, biofuel, ethanol, modelling, pitting corrosion, simulation

Abstract

Bei kraftstoffführenden Bauteilen, insbesondere bei Kraftfahrzeuganwendungen, die bei hohen Temperaturen betrieben werden, wird die Haltbarkeit von Leichtmetallen wesentlich durch ihre Anfälligkeit für Alkoxidkorrosion

beeinflusst. Die Alkoxidkorrosion zeichnet sich durch ihren spontanen Charakter und die außergewöhnlich schnelle Zersetzung der Werkstoffe aus, sobald sie einmal begonnen hat. In dieser Studie wird ein innovativer Hochdruck- und Hochtemperatur-Mikroreaktor vorgestellt, der präzise Messungen mit hoher Empfindlichkeit zur Bestimmung der genauen Initiierungszeiten und Reaktionsgeschwindigkeiten der Lochfraßkorrosion ermöglicht. Es wurden exemplarische Tests zur Untersuchung der Auswirkung von Oberflächenrauheit und Wassergehalt auf die Initiierungszeit von Lochfraß durchgeführt und Daten für ein numerisches Phasenfeldmodell erzeugt, um die Möglichkeiten des Reaktors zu demonstrieren. Vor allem Verunreinigungen auf der Materialoberfläche und im Kraftstoffgemisch haben einen erheblichen Einfluss auf die Korrosivität und damit auf die Zuverlässigkeit der Komponenten. Darüber hinaus wurden die experimentellen Datenpunkte genutzt, um die Korrosionskinetik einzelner Korrosionslöcher zu extrahieren und die numerische Berechnung zu kalibrieren. Die ersten Ergebnisse zeigen, dass es möglich ist, die Korrosionskinetik nachzubilden, die Morphologie der Korrosionslöcher genau darzustellen und reaktionsbezogene Parameter zu schätzen.

SCHLÜSSELWÖRTER
Aluminiumlegierung, Biokraftstoff, Ethanol, Lochfraßkorrosion, Modellierung, Simulation

1 | INTRODUCTION

The alarming issue of global warming has led to intense political and scientific concerns in the past decade. Several guidelines such as the Paris agreement on the global scale, the RED I/REDII on the European Union level or the respective state renewable energy standards in the USA outline a pathway for reducing greenhouse gas emissions. As far as transportation sector is concerned, these guidelines point to a necessary paradigm shift from fossil crude oil products to renewable fuels. In this respect, advanced biofuels such as cellulosic ethanol derived primarily from lignocellulosic biomass, are viable energy alternatives for spark-ignition engines of the transportation sector [1]. Presently, bioethanol is already blended with conventional gasoline, for example 10% v/v in Germany (DIN EN 15376), 15% in the USA (ASTM D4806) or even as high as 27% (RenovaBio Program) in Brazil [2–4]. In addition, another possibility of emission reduction lies in improving vehicular efficiency with stronger and lighter constructions. Thus, aluminium is a preferred material for automotive components with a high strength-to-weight ratio, recyclability, cost-effective large-scale manufacturability (machining, forming) and diverse choice of alloying elements [5]. However, aluminium when used in contact with water-free ethanol fuels is highly susceptible to pitting corrosion at higher temperatures, known as alkoxide or alcoholate corrosion [6–9].

1.1 | Alcoholate corrosion of aluminium alloys

This kind of chemical 'dry corrosion' takes place in alcohols with low water content at temperatures above 80 °C mostly in form of circular corrosion pits and the corrosion reaction is particularly rapid capable of causing component failures in few minutes. Moreover, alcoholate corrosion, due to low electrical conductivity of electrolyte (ethanol), is believed to be a predominantly chemical kind of reaction, which highly depends on physical, chemical and physico-chemical factors such as: water content, temperature, presence of certain alloying elements in aluminium, ethanol impurities and the (metallic) surface condition [10–15]. Equations (1–3) give an overview on the involved reactions [16]:

$$3\ C_2H_5OH + Al \rightarrow Al(C_2H_5O)_3 + \frac{3}{2}H_2 \quad (1)$$

$$Al(C_2H_5O)_3 + 3\ H_2O \rightarrow Al(OH)_3 + 3\ C_2H_5OH \quad (2)$$

$$2\ Al(C_2H_5O)_3 \rightarrow Al_2O_3 + 6\ C_2H_4 + 3\ H_2O \quad (3)$$

At the start of corrosion, once the passive oxide layer is damaged or penetrated by the electrolyte, underlying aluminium reacts directly to form so called alcoholates or alkoxides ($Al(C_2H_5O)_3$); these can further be hydrolyzed to form either gel-like aluminium hydroxide ($Al(OH)_3$) or powder-like aluminium oxide (Al_2O_3). Furthermore, it should be noted that this reaction is exothermic and large amounts of hydrogen is released as the reaction progresses. Thus, the combined involvement of temperature and pressure changes requires this reaction to be studied with special reactors or autoclaves.

1.2 | Definition of problem

In northern America, there exist several norms in order to test for corrosion in biofuels, e.g. NACE Standard TM0172-200 or ASTM D7577 [17, 18]. These norms are, however, beneficial only for 'a qualification' of steels to be used with biofuels based on a numbering system between 1 to 5. They do not address the use of light metals (such as aluminium, magnesium) and the occurrence of alkoxide corrosion. Past research on alcoholate corrosion largely focuses on passive film breakdown mechanisms, the impact of impurities/ions or the ambient medium temperature required for corrosion to occur [6–8, 11, 13, 15, 19]. Although these studies provide a qualitative characterization of the involved reaction, a reliable simulative approach requires more quantitative information starting with time dependent resolution of initiation times and the proceeding reaction kinetics. Consequently, the present work focuses on tailoring previously used experimental reactors/methods to deliver the essential parameters for developing a suitable method to simulate this corrosion mechanism and to analyze experimental data [20]. This work is therefore largely divided into 4 sections:

1. Conducting preliminary tests using available equipment to define its shortfalls in delivering necessary results,
2. Based on these preliminary tests, optimizing the test equipment (micro-reactor),
3. Validating the new experimental set-up (micro-reactor),
4. Efficient use of results for numerical model creation and simulations.

2 | EXPERIMENTAL PROCEDURE

The preliminary tests were conducted using commercially available pure aluminium (Al) according to EN AW 1050A or UNS A91050 having 99.5 % purity with the main alloying elements or impurities being iron 0.32 %, silicon 0.06 %, manganese 0.04 %. Identical test specimens (50 mm×10 mm×5 mm) were cut along the rolling direction. To achieve a homogenous technical surface, all sides of the specimens were prepared by mechanical grinding using a well lubricated silica wheel of grit P1000 at a considerably low speed, avoiding silica embedment on the surface.

High-pressure autoclaves made from stainless steel UNS S31635 (316 titanium) were implemented to conduct the necessary experiments, Figure 1. Due to the titanium content, the reactor material can be considered chemically resistant for the favored fuels. For each experiment, a freshly ground aluminium specimen was placed in a reactor using polytetrafluoroethylene holders. Pre-grinding of samples before each experiment ensured a uniform oxide layer as a starting condition. After sample placement, the reactor was tightly clamped together guaranteeing the required pressure tightness. High purity anhydrous ethanol was used for the experiments ($\geq$ 99.9 %) containing 0.03 ± 0.01 V/V % water, measured using Karl-Fischer titration. For each experiment, 200 ml of ethanol was directly loaded using dosing equipment, from the bottle to the closed reactor, through the pressure relief valve. As ethanol is known for its

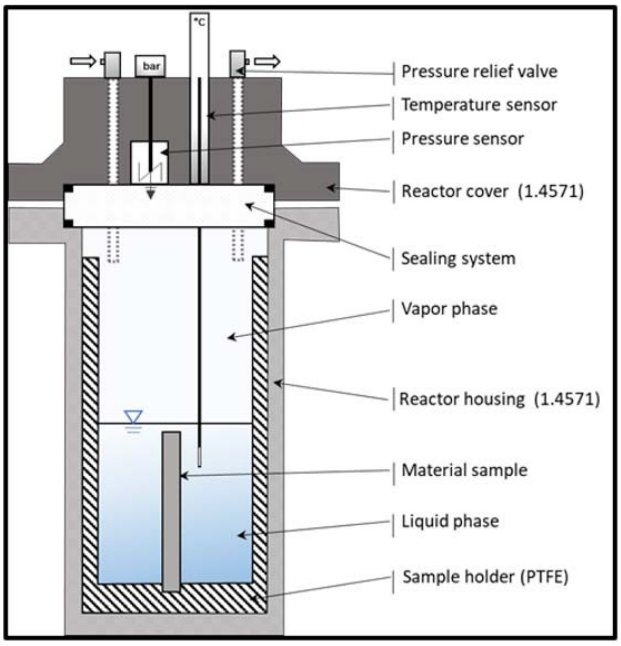

FIGURE 1 High-temperature and high-pressure autoclave used for pre-tests.

water affinity, this method established a uniformity and extremely low water contamination in every experiment. During the test, pressure and temperatures (reactor wall as well as bulk medium) were periodically recorded at a sampling rate of 15 s with an accuracy of ±0.1 bar and ±1 °C respectively.

At the start of experiment, temperature, pressure, and time are defined in the logical controller. A heating time of about 30 minutes is observed after the start of the experiment, Figure 2. Once the required test temperature is achieved, after an activation time, reaction start was indicated by a steep rise in internal temperature and pressure. The rapid pressure change related to hydrogen evolution indicates a rapidly proceeding sample degradation. Thus, to be able to have analyzable samples after tests, the reaction must be manually aborted using the release valve when a certain pressure difference is generated between the ethanol vapor pressure and the reactor pressure (due to hydrogen evolution) calculated with the help of Antoine's equation [21]. Lastly, at the end of experiment, the specimen is cleaned using concentrated nitric acid (68 V/V %), weighed (±0.1 mg) and photographed using optical microscopes. Pit analysis is conducted using optical microscopy followed by image processing using thresholding, binary conversion, and particle analysis using the ImageJ software.

For later validation tests in developed micro-reactors, round samples of 15 mm diameter and 5 mm thickness were used. Similar to above mentioned tests, samples are exposed parallel to rolling direction. Samples were first completely sealed in hot water bath at 100 °C for an hour and dried. Before the tests, only the surface to be analyzed was ground with a 1000 grit paper.

3 | RESULTS

3.1 | Preliminary tests

In an attempt to determine the most important characteristics of alcoholate corrosion for development of a new autoclave, a series of pre-tests were conducted using the present equipment, Figure 1. The parameters were then varied via DoE, Table 1.

Visual inspection shows a mixed pit density with varied surface roughness at constant volume ratio, and identical results are also observed for varied ethanol volume per unit surface area of sample, Table 2. Despite the fact that more than 70 tests were conducted to study

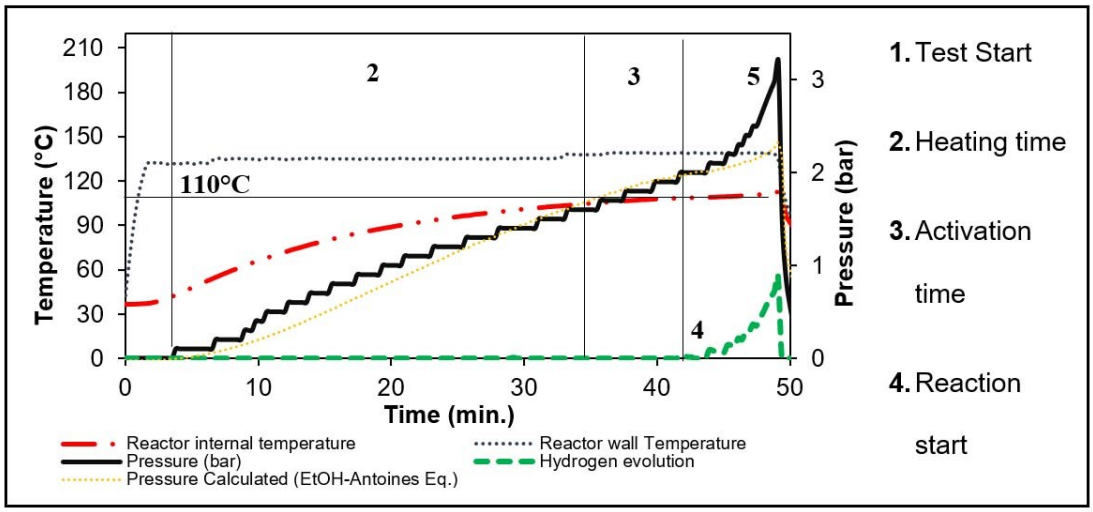

FIGURE 2 Typical progress of an alcoholate corrosion reaction with different time frames.

TABLE 1 Tractional DoE-based test matrix for preliminary tests.

Parameter	Temperature (°C)	Surface roughness (Grit/Ra μm)	Ethanol volume (ml)*	Sample size (mm)*	Electrolyte volume to surface area ratio (ml/mm²)*
Varied values	90	1000 (0.25 ± 0.1)	50	100×10×5	0.8
	100	2500 (0.15 ± 0.1)	200	50×10×5	0.5
	110	4000 (0.04 ± 0.1)	350	10×10×5	0.2

*Volume to surface area is based on varying sample sizes and ethanol volumes.

TABLE 2 Effect of surface roughness and EtOH volume-surface ratio on pitting densities. (Shown size 10 mm×10 mm).

Surface roughness (R_a) (same volume surface ratio)		Volume to sample surface ratio (ml/mm²) (same surface roughness)	
0.04 µm		0.1	
0.14 µm		0.5	
0.24 µm	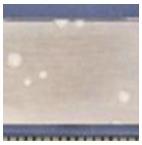	0.9	

these effects, it is still difficult to find any pitting patterns.

A plot of the corrosion initiations or activation times based on varied volume/surface ratios indicated a chaotic distribution which could not be resolved using the present equipment. On the other hand, with an increased sample surface roughness, an upside scattering of the activation times was seen, Figure 3.

3.2 | Effect of grain orientation

The tested specimens were found be differently pitted depending on the sample rolling side. A deeper analysis of the grain structure using electron backscattering diffractometry revealed long deformed grains in the direction of rolling and much smaller flattened grains perpendicular to the rolling direction. Pit population was much higher on the side with smaller grains, Figure 4. Despite the fact that the two faces presented completely different pitting behaviors, no direct correlation between the microstructure and pit initiation was observed. Nevertheless, this gives an indication to the fact that reliable analysis and generation of data for simulation models can occur only with the consideration of just one face (homogenous grain geometry). This is not possible in the present apparatus, Figure 1.

3.3 | Micro-reactor cevelopment

The results from the preliminary tests make it evident that most importantly a higher sensitivity and precision must be required from the new reactor. Moreover, only one sample surface should be tested in the experiments (same grain orientation), with a fixed surface roughness and ethanol volume-surface ratio with a uniform heat distribution on the complete sample surface. Lastly, the reactor should be able to stop the exothermic reaction immediately on set pressure levels (H_2 pressure or corrosion degree). Based on these characteristics initial design considerations were taken, ranging from square type rectors to tube type vessels. The designs were then analyzed based on safety, modularity, precision, complexity and

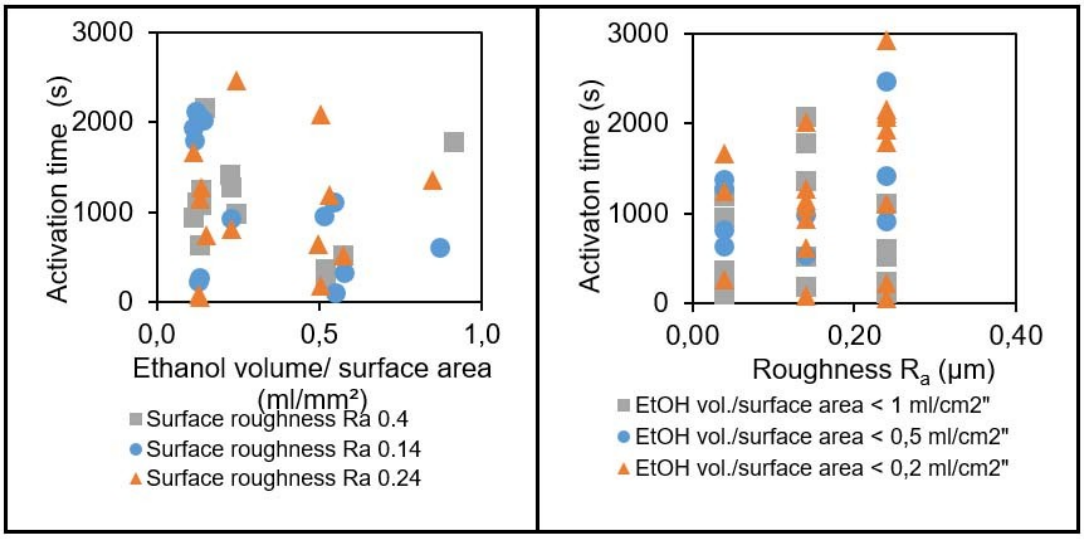

FIGURE 3 Dependence of activation times on (left) ethanol volume to exposed surface area (right) surface roughness.

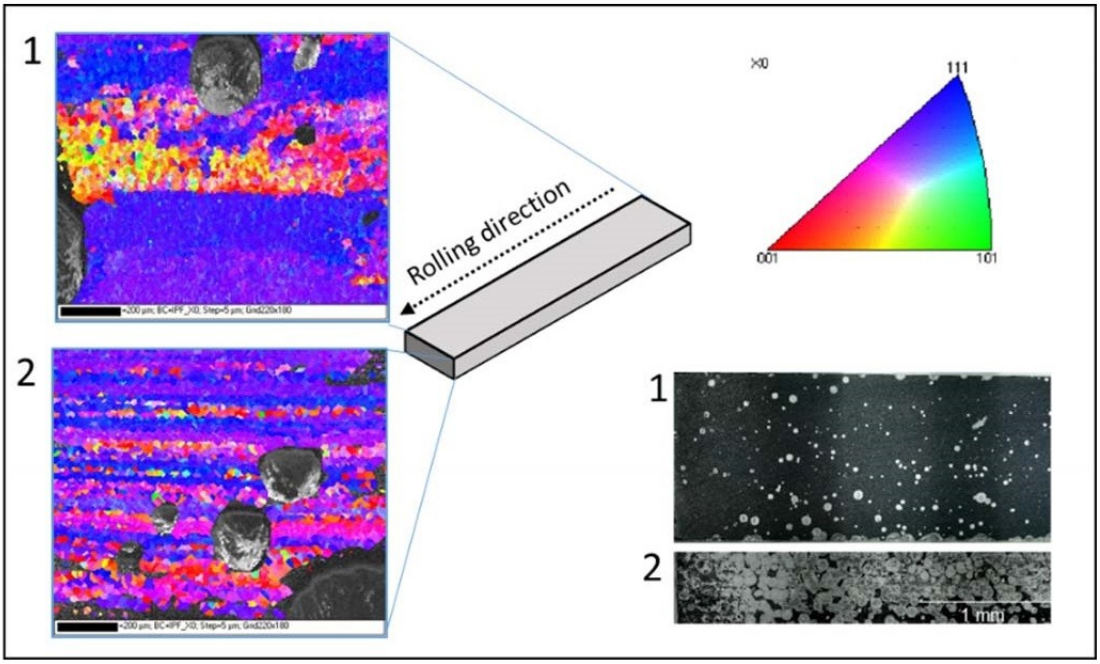

FIGURE 4 Effect of grain structure on the pitting behavior on the face (1) Parallel to rolling direction (2) Perpendicular to rolling direction.

costs according to German guideline TÜV AD-2000 and a relevant design choice was made, Figure 5 [21].

This design was further extended based on the generated criterions from the preliminary tests and the experience gained. Each criterion was evaluated and the requirements were fulfilled by incorporating the necessary design changes, Table 1.

The above design implementation was used and the final design of the reactor was studied by computer simulations, with the focus on heat distribution. The simulations evidenced a constant heat distribution on the sample surface, Figure 6. The construction was completed with stainless steel 1.4571 (UNS31635) and the sealing rings were made from polytetrafluoroethylene to ensure chemical resistance against the reacting media. For the in situ monitoring of reactions taking place, a specially constructed sapphire sight glass was used.

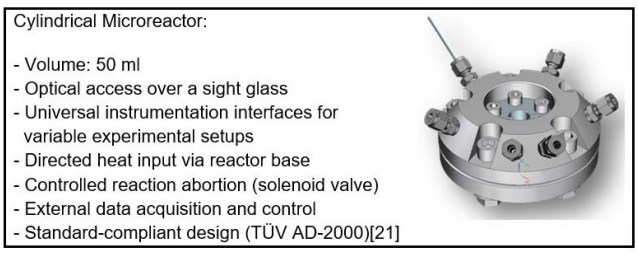

FIGURE 5 Chosen reactor concept.

3.4 | Validation tests

3.4.1 | Surface condition and inhibiting water threshold

Several tests were conducted in order to provide a reliable validation for the new reactor. Here, as an example, the tests involving surface condition and the inhibiting effect of water is shown. Surface preparation methods and the resulting surface conditions can play a major role in nucleation and building of oxide layer or passivation characteristics, residual stresses, or even influencing defect sites, all of which directly has an influence on corrosivity [23]. Furthermore, industrial grinding media, normally composed of silicon carbide crystals can easily embed or be cold welded into soft materials like pure aluminium through grinding which in turn can also cause local stresses in the oxide layer. A test matrix of six different silicon carbide grinding grades were chosen for this analysis, on aluminium AA 1050, Table 3. The calculated vapor pressure for ethanol at 120 °C is circa 5 bar (Antoine equation), 10 bar stop pressure was chosen which allowed 5 bar partial pressure from hydrogen evolution. With stochiometric calculations from Equation (1–3), this led to about 0.25 g mass loss in the samples after experiments, ideally delivering samples with analyzable degradation.

Corrosion incubation temperatures were recorded for each sample (each with 5 repetitions) in pure, nearly

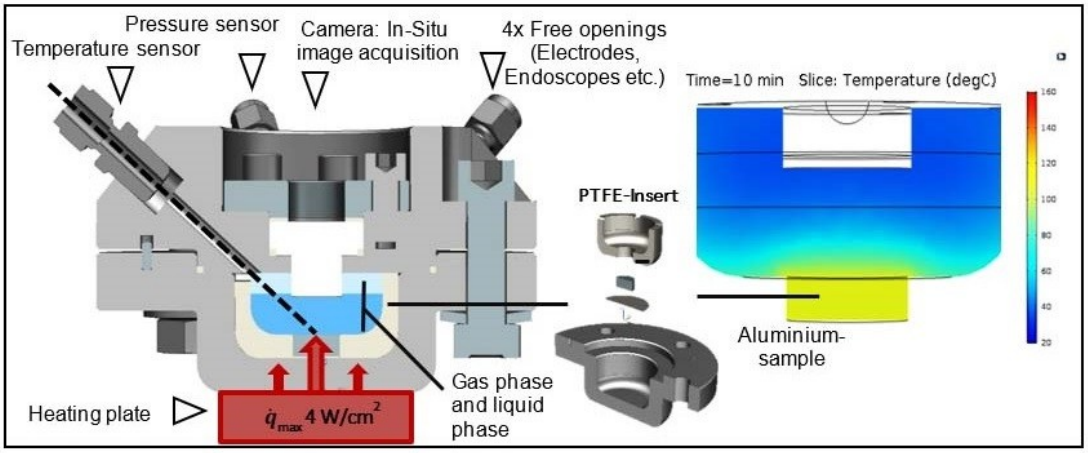

FIGURE 6 Constructed micro-reactor with instrumentation (left). Exemplified heat distribution upon heating (right).

TABLE 3 Test matrix to evaluate surface effects.

Nr.	Sample	Temperature [°C]	Release pressure [bar]	Roughness Ra [μm]	Grinding [grit]
1	01	120	10.0	2.00	180
2	02	120	10.0	0.80	320
3	03	120	10.0	0.40	500
4	04	120	10.0	0.24	1000
5	05	120	10.0	0.14	2000
6	06	120	10.0	0.04	4000

water-free ethanol (SeccoSolv), Figure 7 (left). With an increasing surface roughness, a prevalent decrease in incubation temperatures was seen up to a temperature of about 100 °C. On the other hand, highly polished (4000 grit) samples saw an incubation only in temperature range of approximately 110 °C to 120 °C. This phenomenon was also previously reported for the corrosion of 6XXX aluminium alloys, and it was postulated that corrosion initiation essentially takes place in succession to dehydration of boehmite to aluminium oxide. This dehydration causes a volume contraction in oxide layer leading to high local strains at sites of inclusions causing crack generation and exposure of underlying metal [24]. This dehydration in present system can take place above

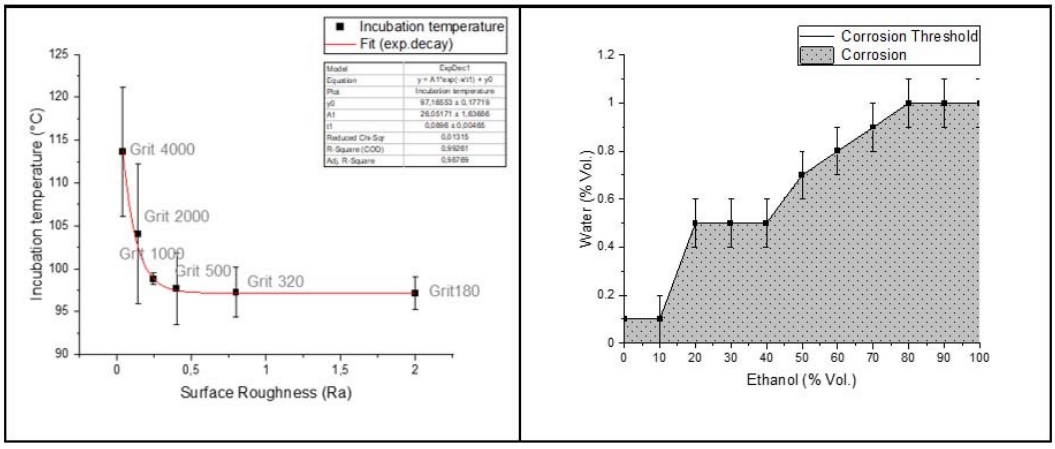

FIGURE 7 (Left) Incubation temperature based on surface roughness, (Right) Limits for water content for reaction inhibition at 150 °C.

a temperature of 100 °C, which is similar to the observed results. The exponential increase in initiation temperatures with lower roughness, can also be directly correlated to the size of cold welded silicon carbide inclusions on aluminium. In comparison to earlier results, much reliable analysis could be achieved with the new equipment, Figure 3.

Second part of validation tests involved finding an absolute threshold of water required depending on ethanol-gasoline blend content. It is a known fact that water plays an inhibiting role in corrosion of aluminium in ethanol [6–8]. Technological threshold for inhibiting water contents were previously reported to be around 1250 ppm (0.12% V/V), 3500 ppm (0.35% V/V), and 3500 ppm (0.35% V/V) for AA 1050 in E10, E25, and E80 at 120 °C [25]. In present study, E0 to E100 was analyzed, with a 10% V/V steps including a chloride content of 10 ppm at 150 °C for a maximum duration of 3 days. Water contents in blends was increased in 0.1% V/V steps until a corrosion inhibition was achieved. Each test was repeated 3 times. Results show a strong trend for water contents, Figure 7 (right). A water content of 0.1% V/V is sufficient to cause inhibition in E10 fuels, also comparable to previous studies. A slightly parabolic increase in water content is noticed, with a plateau at 1% V/V starting at E80 and a slight plateau between E20 and E40. Further tests are being conducted with varying chloride content to completely understand the shifts in inhibiting water contents.

3.5 | Simulation approach to alcoholate pitting corrosion

3.5.1 | Preliminary considerations

In previous observations, it was noted that random initiation events of pits occur on the surface of the substrate when a critical temperature is reached, Figure 4. By utilizing micro-reactor experiments and video recordings, it was possible to observe the growth process. During this growth phase, hydrogen bubbles form rigorously inside the pit causing buoyancy. This observation is significant as it supports the assumption of a chemical corrosion reaction involving separate anodic and cathodic half-reactions. Consequently, the phenomenon of metastable pitting, where pits cease to grow due to the absence of a sustained aggressive environment within the pit which is frequently observed in electrochemical corrosion scenarios could not be observed. Thus, a purely chemical process is assumed as driving mechanism.

Another noteworthy finding pertains to the behavior of the passive layer during the corrosion reaction. In certain metals like iron, the formation of lace-like covers occurs above the growing pits in acidic aqueous electrolytes. This means that the protective oxide layer only partially breaks down, impacting ion transport within the pit and, consequently, the pit's shape [26]. Based on our experimental observations, it can be asserted that complete breakdown of the passive layer occurs during growth in the case of AA1050 pitting corrosion in anhydrous ethanol. This finding holds particular importance as it provides crucial input for subsequent simulations. The hydrogen evolution from within the pit is believed to facilitate the detachment of the passive layer, which explains this observation. It should be noted that the formation and buoyancy of hydrogen bubbles in the solution may result in significant convective fluxes that influence mass transport. Consequently, the consideration of this two-phase flow phenomenon necessitates dedicated additional experimental and modelling efforts, which will be considered in upcoming studies.

3.5.2 | Growth process

During pit growth, the time dependent pit shape can give indications towards the underlying reaction mechanism. In particular, the ratio of observed lateral and depth kinetics is determined by the extent of diffusion contribution to the dissolution process. These conclusions were drawn and from experiments and simulations for aqueous ferrous alloy systems [27].

In the present experimental set-up, it is possible to observe the time-dependent lateral pit expansion in situ. Pit sizes are plotted for four different temperatures after initiation of the first pit, Figure 8. The slopes of individual pit sizes obey a linear relation ($R^2 \geqslant 0.9$ for all pits) with respect to time which indicates activation-controlled growth mechanism. Moreover, a higher temperature leads to faster growth as expected.

Because the pit depth during the growth phase is undetermined, the depth analysis was conducted post-mortem. The results are plotted for the different temperatures, Figure 9. It is evident that the depth is always smaller than half width which is indicated by calculated slopes of smaller than 0.5. The depth is controlled by diffusion to a greater extent than the width in the analyzed conditions.

3.5.3 | Phase field model

A phase field model was implemented for describing the pitting corrosion growth process. The model is based on previously established Kim-Kim-Suzuki (KKS) phase

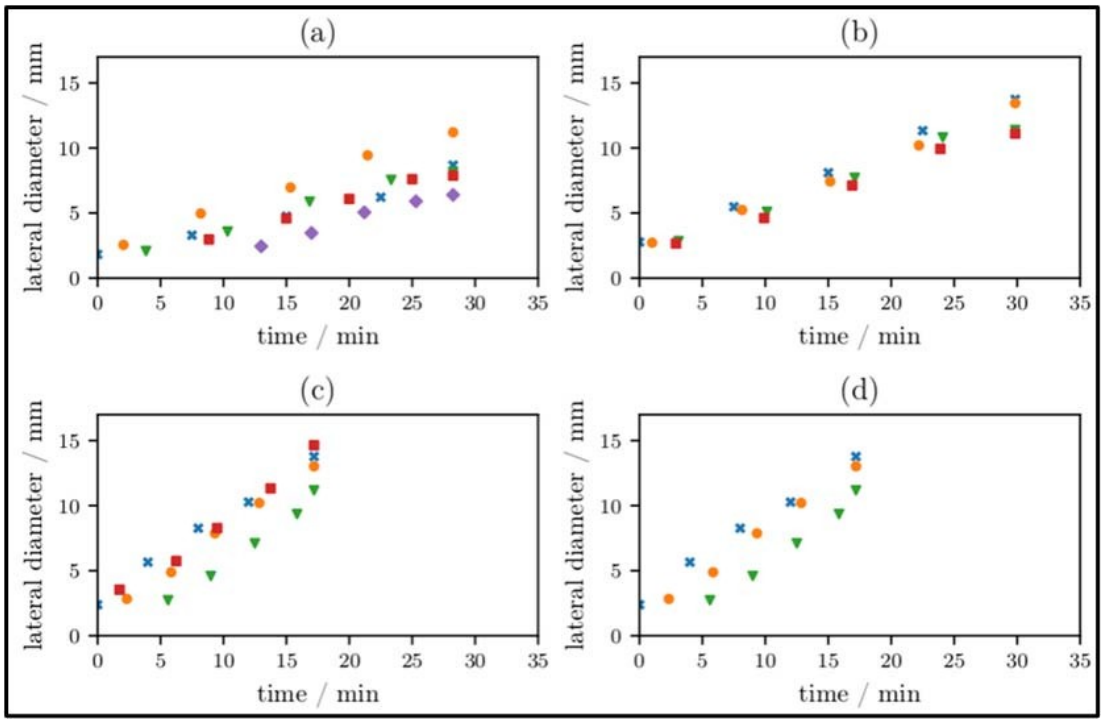

FIGURE 8 Lateral pit size expansion for (a) 95 °C, (b) 100 °C, (c) 110 °C and (d) 120 °C of AA1050 in anhydrous ethanol. At least three pits were measured for each temperature.

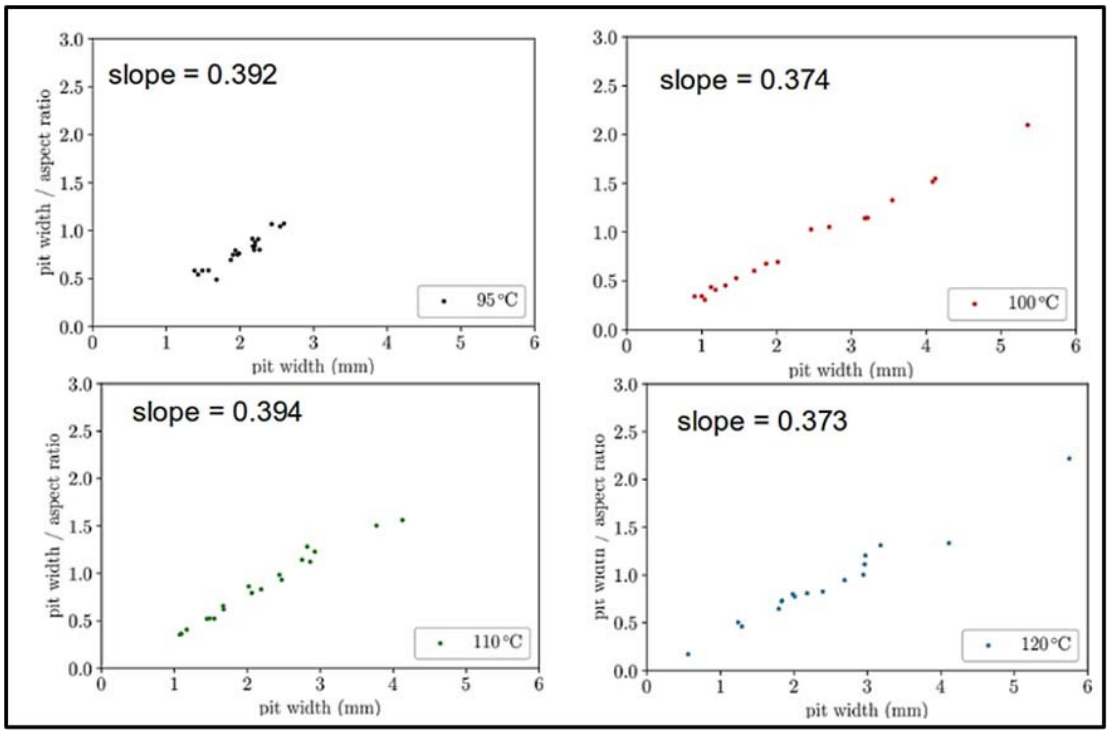

FIGURE 9 Pit aspect ratio vs pit width for the four examined temperatures with fitted linear slopes.

transformation models [28, 29]. The reader is referred to the cited publications for more details.

The governing equations were implemented using finite element method (FEM) with six-node triangular Lagrangian elements for space discretization and backward differentiation formula (BDF) for time integration. An axisymmetric simulation domain of 10 mm×20 mm was created with a 10 mm×10 mm for

the liquid and solid domain respectively. An opening of 0.1 mm was placed in between the domains introducing a very narrow (0.1 mm) domain on both sides of the opening which mimics the passive layer. At minimum 8 elements are allocated in the transitional region for precise calculation of the order parameter gradient and numerical stability. Initial conditions were: $c'=0$ and $\eta=0$ in the electrolyte domain and $c'=1$ and $\eta=1$ in the alloy. Natural boundary conditions ($\partial c'/\partial n=0$ and $\partial\eta/\partial n=0$) were applied at all outer boundaries.

The model allows an estimation of kinetic parameters, in this case the activation energy of the chemical reaction (E_A), by calibrating the parameters so that the observed pit sizes are obtained at given temperatures. The pit size and especially the pit aspect ratio is governed by the activation vs diffusion mode of the process. The order parameters c' and η evolve according to the Allen-Cahn (4) and Cahn-Hillard (5) equations, respectively:

$$\frac{\partial\eta(\mathbf{r},t)}{\partial t}=-L_\eta\left(\frac{\delta\mathcal{F}}{\delta\eta}-\alpha_\eta\nabla^2\eta(\mathbf{r},t)\right) \tag{4}$$

$$\frac{\partial c'(\mathbf{r},t)}{\partial t}=\nabla\cdot\kappa\nabla\left(c'(\mathbf{r},t)-h(\eta)(c_{se}-c_{le})-c_{le}\right) \tag{5}$$

where $L\eta$ is correlated to the reaction kinetics, $\mathcal{F}$ is the free energy, α_η is an interfacial coefficient governing the interface thickness in the phase field, and κ is related to the diffusion coefficient of the metal ion in the liquid phase. c_{se} and c_{le} are the equilibrium concentrations of Al in solid and liquid, respectively. The temperature dependence of the diffusion coefficient is governed by the Stokes-Einstein relation whereas the kinetics obey the well-known Arrhenius equation. Diffusion control of the reaction is introduced by defining a temperature-dependent solubility constant of the forming aluminium ethanolate salt as available in literature [30]. The pit growth data in pure ethanol without impurities and subsequent microscopic analysis was utilized to determine the kinetic coefficients. Further details of developed the phase field model will be published in a subsequent paper.

The pit evolves to an ellipsoidal shape like observed in experiments after a 5 min reaction time at 110 °C, Figure 10. The resulting pit to depth aspect ratio at different temperatures and reaction times was compared to measured values to validate the model, Figure 11. The model is able to reproduce the pit shapes and sizes at the given conditions with reasonable accuracy after calibration of parameters (kinetic coefficient $L\eta$ and mobility coefficient κ).

The calibration of the model was performed by conducting parametric studies. From these, an activation

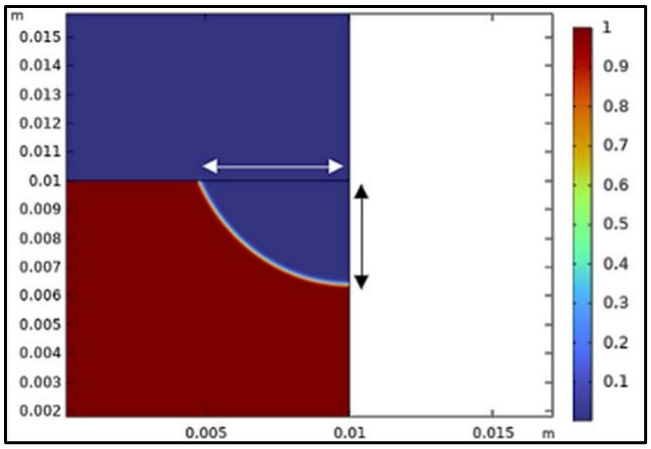

FIGURE 10 Exemplary simulation result of η (color) on the geometry (x and y) after $t=5$ min at $T=110$ °C.

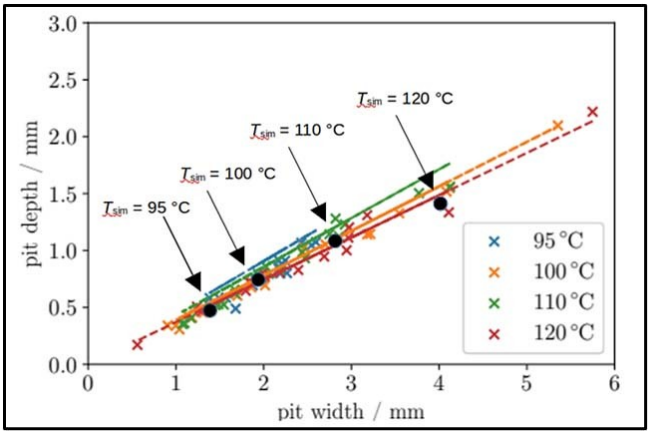

FIGURE 11 Experimental pit to depth ratio at different temperatures and simulated pit shapes at $t=10$ min (black dots).

energy $E_A=-78.5\ \mathrm{kJ\,mol^{-1}}$ and a diffusion coefficient $D_{Al,25\,°C}=0.5\cdot10^{-9}\ \mathrm{m^2\,s^{-1}}$ was estimated.

To sum up the section, it was shown that the chemical pitting corrosion reaction of AA1050 in anhydrous ethanol can be analyzed by the novel experimental setup. It facilitates a top-down determination of the reaction mechanism and estimation of decisive reaction kinetics and diffusion parameters. Next steps include the addition of water-related terms into the model which will enable an overlapping electrochemical mechanism.

4 | DISCUSSION OF RESULTS

Due to the statistical nature of pit initiation in case of thermally induced passive layer breakdown, the necessity of a precise thermal input is evident to produce reliable results. In electrochemically induced pitting

corrosion, experimental conditions are usually set by a high-precision potentiostat that can turn on the potential or electrical current in a matter of milliseconds. This level of precision is, obviously, not possible with a thermal reaction control but a certain increase in accuracy and correspondence between apparent and real incubation and reaction time can be achieved by decreasing the reaction volume. However, a small reaction volume can negatively affect the heat dissipation in case of exothermic reaction which is present in this case. A faster (undesired) temperature increase is expected in the occluded volume. Nonetheless, the newly developed microreactor still produced more accurate results which proves the feasibility of the chosen approach. Regarding the water content necessary to inhibit the corrosion onset, similar trends like reported in literature for AA1050 but with less experimental effort indicate a superior performance of the constructed reactor.

Moreover, the employment of the novel reactor clearly shows the chemical nature of the alkoxide corrosion reaction. This means, that initiated pits grow independently from each other without phenomena like metastable pitting. This enables a precise prediction of time-dependent damage penetration and estimation of reaction kinetics which was not previously reported for alkoxide corrosion. The results can be used in future research to evaluate the effects of further electrolyte additives on growth kinetics of singe pits.

5 | CONCLUSIONS

An experimental procedure was devised with the capability of delivering reliable results in order to produce simulative models for predicting material degradation due to alcoholate corrosion. The following can be concluded as a summary:

1. Pre-tests showed the shortfalls of present testing equipment in delivering time dependent corrosion kinetics required for a simulative model or quantitative analysis.
2. A new micro-reactor was constructed, specifically tailored to enable precise analysis of thermally induced alcoholate corrosion reaction and the kinetic characteristics.
3. A phase field simulative approach was suggested. The chemical pitting corrosion reaction of AA1050 in anhydrous ethanol can be analyzed by the experimental set-up. It facilitates a top-down determination of the general reaction mechanism and estimation of decisive reaction and diffusion parameters.
4. Validation tests conducted in the new equipment, combined with the simulation technique show promising results.

Present technique can further be applied to practice related aluminium alloys and bio-fuel blends in order to predict the lifetime of automobile components. Moreover, the authors intend to further improve the experimental apparatus to be able to conduct high temperature thermography and electrochemical studies. Furthermore, factors such as water and impurities are being inculcated in the model. The research progress will be reported in future publications.

ACKNOWLEDGEMENTS

The authors would like to thank the Deutsche Forschungsgemeinschaft/German Research Foundation (DFG) for their financial support during the projects AlKoMo I/II: *Alcoholate Corrosion: Critical damage mechanisms and their progression identified and described via experiment and modelling* (DFG HO4478/6-1, OE558/20-1, DFG HO4478/6-2, OE558/20-2).

Correction added on 24 September 2024, after first online publication: Projekt Deal funding statement has been added.

Open access funding enabled and organized by Projekt DEAL.

CONFLICT OF INTEREST STATEMENT

The authors declare no financial or commercial conflict of interest.

DATA AVAILABILITY STATEMENT

The data that support the findings of this study are available from the corresponding author upon reasonable request.

ORCID

E. Gazenbiller http://orcid.org/0000-0002-6361-4275

REFERENCES

1. S. Kusch, presented at 17th International Multidisciplinary Scientific GeoConference SGEM2017, June 20, **2017**.
2. Standard DIN EN 15376:2014-12, *Deutsches Institut für Normung e.V.*, **2014**.
3. Standard ASTM D4806-20, American Society for Testing and Materials, **2020**.
4. S. Barros, Brazil Biofuels Annual, *United States Department of Agriculture*, **2019**.
5. J. Zehnder, R. Pritzlaff, S. Lundberg, B. Gilmont, Aluiminium im Nutzfahrzeugbau, *European Aluminium Association*, **2011**.
6. Jenny Linder, *Master thesis*, KTH Royal Institute of Technology, **2012**.
7. R. Reitz, *Doctoral thesis*, TU Darmstadt, **2019**.

8. R. Reitz, G. Andersohn, M. Oechsner, *Matwiss. Werkstrofftech.* **2016**, *5*, 140.
9. F. Tuchscheerer, L. Krüger, M. Mandel, S. Müller, S. Liebsch, *Matwiss. Werkstrofftech.* **2013**, *44*, 555.
10. M. Pourbaix, R. W. Staehle, *Lectures on Electrochemical Corrosion*, Springer, US, **1973**.
11. K. Eppel, M. Scholz, T. Troßmann, C. Berger, *Energy Mater.* **2008**, *3*, 227.
12. G. R. Kramer, C. M. Méndez, A. E. Ares, *Mater. Res.* **2016**, *21*.
13. L. Krüger, F. Tuchscheerer, M. Mandel, S. Müller, S. Liebsch, *J. Mater. Sci.* **2012**, *47*, 2798.
14. T. Tsuchida, *Corros. Eng.* **2004**, *53*, 44.
15. M. Scholz, J. Ellermeier, *Matwiss. Werkstofftech.* **2006**, *37*, 842.
16. C. Vargel, *Corrosion of Aluminium*, 1st ed. Elsevier: Amsterdam, **2004**.
17. Standard test method NACETM0172-2001, *NACE*, **2001**.
18. Standard test method ASTMD7577-12, *ASTM*, **2021**.
19. M. Hück, *Matwiss. Werkstofftech.* **1994**, *25*, 20.
20. E. Gazenbiller, V. Arya, R. Reitz, T. Engler, M. Oechsner, D. Höche, *Corros. Sci.* **2021**, *179*, 109.
21. G. Thompson, *Chem. Rev.* **1946**, *38*, 1.
22. Richtlinien AD 2000-Code, *TÜV AD*, **2020**.
23. S.-S. Wang, F. Yang, G. S. Frankel, *J. Electrochem. Soc.* **2017**, *164*, C317.
24. L. Calabrese, P. Bruzzaniti, E. Proverbio, *Mater. Corros.* **2018**, *69*, 1815.
25. G. Andersohn, R. Reitz, M. Oechsner, presented at *NACE 2014*, San Antonio, USA, **2014**.
26. P. Ernst, N. J. Laycock, M. H. Moayed, R. C. Newman, *Corros. Sci.* **1997**, *39*(6), 1133.
27. S. Scheiner, C. Hellmich, *Comput. Methods Appl. Mech. Eng.* **2009**, *198* (37–40), 2898.
28. T. Q. Ansari, Z. Xiao, S. Hu, Y. Li, J.-L. Luo, S.-Q. Shi, *NPJ Comput. Mater.* **2018**, *4*, 1.
29. W. Mai, S. Soghrati, *Electrochim. Acta* **2018**, *216*, 290.
30. W. Wang, T. Zhang, Y. Wang, W. Tang, *J. Chem. Eng. Chin. Univer.* **2015**, *6*, 1293.

How to cite this article: V. Arya, E. Gazenbiller, R. Reitz, M. Oechsner, D. Höche, *Materialwiss. Werkstofftech.* **2024**, *55*, e202300244.
https://doi.org/10.1002/mawe.202300244